On Non-linear rotor dynamic effects of aerodynamic bearings with simple flexible rotors

Benyebka Bou-Saïd, Grégory Grau, Ivan Iordanoff

On Nonlinear Rotor Dynamic Effects of Aerodynamic Bearings With Simple Flexible Rotors

B. Bou-Saïd[1]
Laboratoire de Mécanique des Contacts et des Solides,
Bâtiment Jean D'Alembert 20 Rue des Sciences INSA,
20 Avenue A. Einstein 69 621,
Villeurbanne Cedex, France

G. Grau
Microturbo 8 Chemin du Pont de Rupé BP 2089, Toulouse Cedex 2, 31 019 France

I. Iordanoff
ENSAM-33405,Talence Cedex, France

The last decades have experienced a growing enhancement of aeronautical oil free turbomachinery. The classical linear approach of rotor dynamics commonly uses stiffness and damping coefficients to model journal bearings. In the present study, a nonlinear time dependant calculation is used for the dynamic simulation of a rotor mounted with aerodynamic (gas) bearings. A comparison between the two approaches indicates that the dynamic behavior of such bearings can be nonlinear in operating ranges where the rotor eccentricity reaches high values. In that case, the linear approach may lead to incorrect results and the nonlinear approach should be performed for better rotor dynamic prediction. A numerical procedure which analyzes the dynamic behavior of simple flexible rotors taking into account the nonlinear (transient regime) characteristics of aerody-namic bearings is presented. A simple example highlights the needs of nonlinear simu-lations in order to predict dynamic performance in oil-free turbomachinery.

Keywords: foil bearings, rotor dynamics, stability, gas lubrication

Introduction

The designers of turbine engines have always had to deal with very severe restrictions concerning weight. Consequently, these designers focused on an increase in the specific power involving a reduction in the size of the machines, and an increase in rotating speed. In ranges of 30,000 to more than 100,000 rpm, an aerodynamic (gas bearing) approach seems well adapted compared to the traditional technological elements which cannot meet certain requirements, e.g., those concerning adequate lifetime. Thus air bearings have received considerable attention in these last decades and find increasing applications whenever elevated speeds, low loads, and a high degree of accuracy are necessary.

There are two operating conditions for aerodynamic bearings which are quite distinct: a dry contact-mixed lubrication mode, and an aerodynamic lubrication mode. The first condition corresponds to the transient mode and specifically the start-stop phases. This study deals with the latter behavior, when a complete film of air separating the rotating member from the static member is created. The determination of the pressure field in the bearings from the solution of the Reynolds equation in the case of compressible fluids, in particular with perfect gases, has been intensively investigated [1–3]. Air bearing static behavior has been previously treated by several authors [3–11].

Once static properties are known, designers must investigate the dynamic properties of the system consisting of the shaft and the bearings. In this paper, we will first treat the dynamic behavior of a rigid shaft mounted symmetrically on two aerodynamic bearings. Two methods of calculation, linear and nonlinear, are presented and compared in this simple case. This comparison reveals differences in results according to the loading, particularly in terms of speed instability and response to an unbalance excitation force. This portion of the study will lead us to suspect that the linear approach may be inadequate in some range of operating conditions compared to the nonlinear approach. Next, an improvement taking into account damping within the deformable structure of the bearings is highlighted. The last part of this study enables us to improve our understanding of the dynamic behavior of a deformable shaft by including nonlinear aspects of the problem.

A first model is based on a simplified approach to the problem. The step by step calculation is validated by comparison with the traditional linear rotor dynamics analysis. An improvement of this model is then made possible using the Rayleigh-Ritz method based on three elementary vibration modes taken for the shaft. Thus, we can evaluate the influence of the flexibility of the rotor on its critical engine failure speeds, and also on the level of stability of the system. The encouraging results of this modeling lead us to a more complicated finite element method approach. In our conclusions we will point out the principal results and place the present contribution in context. Finally, some directions of future research will be proposed.

Bump Foil Bearing

Many numerical and experimental studies have been concerned with the static and dynamic characteristics of so-called bump foil bearings. These works are generally concerned with two separate issues:

- Tribological phenomena related to the stop/start phases. Dry friction occurring during these phases is the main cause of deterioration of the bearings. The texture and shape of the surfaces and the materials in contact play a major role in these phenomena [12–15];
- Development of models to predict aerodynamic bearing performance in terms of carrying capacity, power loss and dynamic behavior [3,7,16,17].

This work is a contribution to the second research area. The bump foil technology allows us to take a very simple structural approach to the analysis. The upper foil ensures the continuity of the profile. The geometry of the bearing and the structural behavior are governed by the springs on which the upper foil is pressed, see Fig. 1.

Architecture and Geometry. Bump foil bearings present several alternatives. Indeed, the number of lobes and foils (for which

[1]Corresponding author.

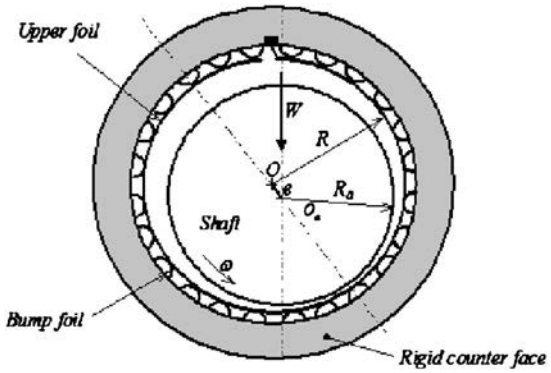

Fig. 1 Bump foil bearing description

the stiffness varies) can be adapted according to the desired performance. The first bearing developed with this technology consisted of a rigid sleeve onto which a corrugated foil and an upper foil are welded extending along all the bearing circumference. This foil assembly determines the general profile of the bearing film and its deformability (Fig. 1).

A correct implementation of the fixed deformable structure of the bearing foil must consider a variation of its structural stiffness with the angular position of the considered point [18]. The characteristics of this type of bearing are very close to its rigid counterpart (a smooth journal bearing) and this allows the bearing to support high loads,[9,19].

Aerodynamic Performance. The literature is replete with numerical and experimental work presenting the static and dynamic performance of foil bearings [19–30]. The description of their behavior follows the same format as for hydrodynamic bearings. However, in addition, one has to take into account the effect of compressibility of the fluid coupled with the structural deformation, i.e., an aero-elastic coupling.

The analysis of the foil bearing dynamic behavior can be carried out according to two different methods. In the linear method, the dynamic coefficients (stiffness and damping matrices) of the bearing are first calculated. Reynolds equation is solved for small increments of relative journal and bearing displacement and velocity, enabling evaluation of these coefficients. These matrices are then used to study the rotor dynamics. [31–34]. With the nonlinear method, the rotor dynamic movements are calculated in a step by step fashion based on the coupled resolution of Reynolds equation. This process gives the forces due to the bearings, and the equations of rotor dynamics [35–38].

The assumption of small displacements of the shaft center inside the bearing causes the linear analysis to have certain limitations. The method assumes that the variation of aerodynamic force with respect to its equilibrium position is nearly linear. A nonlinear analysis calculates the bearing forces at each time step to study the rotor dynamic behavior. No assumptions are needed for the bearing force evolution [30,39,40]. This type of study is rarely presented in the literature of foil bearings because of large computer demands in terms of time and memory [41,42]. On the other hand, similar work with incompressible fluids [35,31,43], confirms the importance of considering this type of analysis in certain operating conditions.

Indeed, some isolated works highlight interesting phenomena on the specifics of the linear and nonlinear approaches [44–46]. According to these works, the linear approach presents a restricted field of validity. It is thus important to investigate this point in order to avoid erroneous results.

Bearing Damping. The phenomena related to damping within the bearing structure are the subject of many numerical and experimental studies. One of the assumptions used in the past to explain the higher damping of the foil bearings is based on the presence of internal friction inside the deformable structure. Consequently, to add damping, some researchers assumed it was sufficient to increase the friction coefficient between the foils by using various types of coatings. Peng and Carpino [47] presented an analytical study in which they showed that damping in air bearings increases when the air film stiffens. As the eccentricity or the load increases the air film becomes stiffer and thus activate the dry friction between the bump and the housing. This phenomenon induces additional damping. They noticed that when the air film is flexible, i.e., when the load is light or the rotational speed is relatively low, ball bearings offer more damping than foil bearings. On the other hand, for higher load and speed, when the film of air is stiff, foil bearings provide more damping than their rigid counterparts due to the damping generated by friction between the foils of the deformable structure [48–50]. Damping can be considered using a viscous model when the load is small and the temperature high. Apparently, the addition of internal friction does not have any notable influence [28].

Table 1 Data input for the lobed bearing

L/D	0.75, 1, 1.25
D	50 mm
Number of pad	3
Pad angle, deg	110
Radial clearance, μm	50

Rotor Model. Classical theoretical studies have been interested in the dynamic characteristics considering the simplified case of a rigid rotor supported symmetrically by two identical bearings. The modeling of the dynamic action of the bearings is performed using the linear approach. Few authors considered the nonsymmetrical problem with a deformable rotor, and no existing study presents the direct coupling (with nonlinear analysis of the bearings) between the dynamic analysis of the rotor and its interaction with the foil bearings.

Comparison Between Linear and Nonlinear Methods

It is interesting to compare the linear and nonlinear methods to determine the range of validity. To this end, results in terms of stability level and unbalance response are given. For simplification, a rigid rotor symmetrically mounted on two identical three lobes rigid bearing is considered. The geometry of the lobes is circular and no geometrical preload is applied. The main characteristics are given in Table 1. The load on the bearing is only that of the rotor mass. For the stability study (Fig. 2), the critical speed is investigated for different rotor mass values. For the unbalance study (Fig. 3), the rotor mass is fixed at 2.25 kg and the mass unbalance is fixed at 1 g mm.

The results presented in Figs. 2 and 3, thus confirm the nonlinear dynamic behavior of the air bearings according to the operating range. Concerning stability, at high loads (corresponding to high eccentricity) the stability threshold given by the linear approach differs from that given by a nonlinear approach. Concerning response to a mass unbalance, there is a transition between the ranges where the two methods are in agreement and where they present strong differences. At high velocity (low values of eccentricity), the two methods give identical results, but they present dramatically different results at low velocity (high values of eccentricity).

However, the differences in phenomena observed concerning the domains of validity of the two approaches remain to be clarified. The definition of the limits of validity of the linear theory is thus a relevant direction of study for aerodynamic bearings. The comparison of the results given by linear and nonlinear approaches, Figs. 2 and 3, highlights the differences between these two methods. The curves obtained are very distinct. These differ-

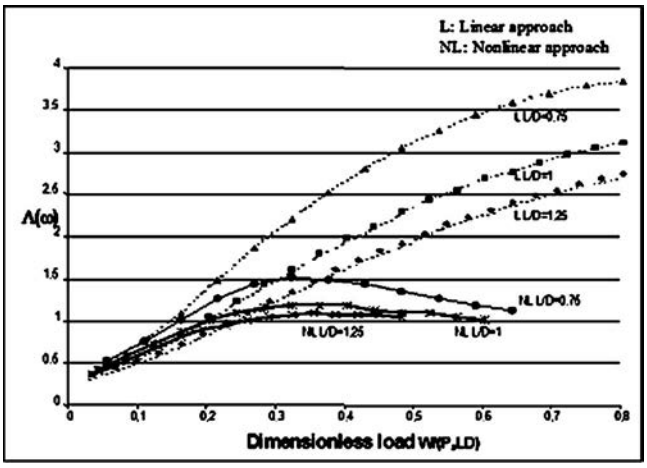

Fig. 2 Evolution of critical speed value against the dimensionless static load

ences occur both in term of stability threshold and response to unbalance. When aerodynamic bearings are highly loaded, it seems to be more accurate to use the nonlinear analysis.

Accounting for Structural Damping

Following the conclusion of the study where we compared the linear and nonlinear approaches, we set up a model taking into account a structural damping similar to that presented for the linear analysis in [51] and [33], but adapted to nonlinear calculation [26].

Modeling. This model has been detailed in [52]. The main idea here consists in rewriting the balance equations for deformable bearings taking into account the speed of deformation. The compressive forces generated in the air film are balanced by forces due to the bearing stiffness (or the compliance S_c) and due to its damping (viscous damping coefficient per unit of area noted C_e), Fig. 4.

Starting from the balance forces on the upper foil the expression of the variation of the pressure field between t and $t+dt$ can be written as

$$(P^{t+dt}-P^t)=\frac{1}{S_c}(H^{t+dt}-H^t)+\mathrm{C_e}\left(\left.\frac{dH}{dt}\right|_{t\to t+dt}-\left.\frac{dH}{dt}\right|_{t-dt\to t}\right) \tag{1}$$

Expressions of the terms dH/dt described previously are as follows:

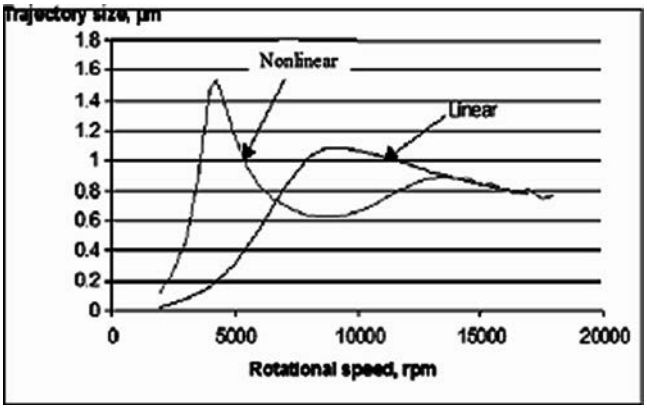

Fig. 3 Comparison of linear and nonlinear approaches

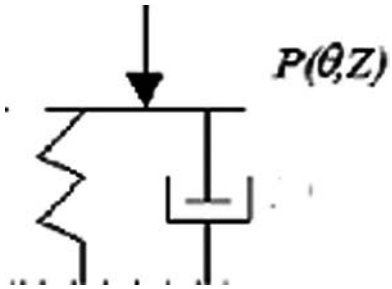

Fig. 4 Sketch of the model

$$\left.\frac{dH}{dt}\right|_{t\to t+dt}=\frac{H^{t+dt}-H^{t+dt}_{\mathrm{save}}}{\Delta t}\quad\text{and}\quad\left.\frac{dH}{dt}\right|_{t-dt\to t}=\frac{H^{t}-H^{t}_{\mathrm{save}}}{\Delta t} \tag{2}$$

where H^t_{save} is the film thickness at time t before deformation, H^t is the film thickness at time t after deformation, $H^{t+dt}_{\mathrm{save}}=H^t$ + displacement of the shaft between t and $t+dt$ (the film thickness at time $t+dt$ before deformation), and H^{t+dt} is the film thickness at time $t+dt$ after deformation. From the above, (1) can be expressed in the following form:

$$(P^{t+dt}-P^t)=\frac{1}{S_c}(H^{t+dt}-H^t)+\mathrm{C_e}\left(\frac{H^{t+dt}-H^{t+dt}_{\mathrm{save}}}{\Delta t}-\frac{H^{t}-H^{t}_{\mathrm{save}}}{\Delta t}\right) \tag{3}$$

Therefore, the relation giving the film thickness can be obtained as

$$H^{t+dt}=H^t+\frac{S\,.\,\Delta t}{\Delta t+S_c\,.\,\mathrm{C_e}}\left(P^{t+dt}-P^t+\frac{\mathrm{C_e}}{\Delta t}(H^{t+dt}_{\mathrm{save}}-H^t_{\mathrm{save}})\right) \tag{4}$$

This film thickness is then introduced in the Reynolds equation in order to obtain the pressure field at each time step,

$$\frac{\partial}{\partial\theta}\left[PH^3\frac{\partial P}{\partial\theta}\right]^{t+\Delta t}+\frac{\partial}{\partial Z}\left[PH^3\frac{\partial P}{\partial Z}\right]^{t+\Delta t}=\Lambda\left(\frac{\partial PH}{\partial\theta}\right)^{t+\Delta t}+2\Lambda\left(\frac{P^{t+\Delta t}-P^t}{\Delta t}H^{t+\Delta t}+P^{t+\Delta t}\frac{H^{t+\Delta t}-H^t}{\Delta t}\right) \tag{5}$$

Influence of Damping on the Threshold of Stability. The structural damping coefficient influence on the stability threshold is then studied using the set up model. The viscous damping coefficient used in the model can be replaced, in an equivalent way, by the damping coefficient used classically in rotor dynamics [53,54],

$$\alpha=\frac{C_e}{2\sqrt{KM}}$$

where: C replaces the viscous damping coefficient C_e, K replaces the reverse of the compliance coefficient S_c, and M represents the mass of the rotor assigned to the bearing.

All the studied profiles of the bearings are with three deformable smooth lobes (Fig. 5) and all the grooves are identical and have an extent of 10 deg (Table 2). We thus have represented the critical engine failure speed diagram for various values of α associated with this profile, Fig. 6. For comparison, we include the curve corresponding to the rigid profile.

It appears clearly that the addition of damping within the deformable structure, brings about a striking increase of the stability level for a compliant bearing (as for the low values of α). As could be expected, the higher the damping coefficient, the higher the critical speed. Furthermore, the critical speed does not decrease further with load increase. The relation between the critical

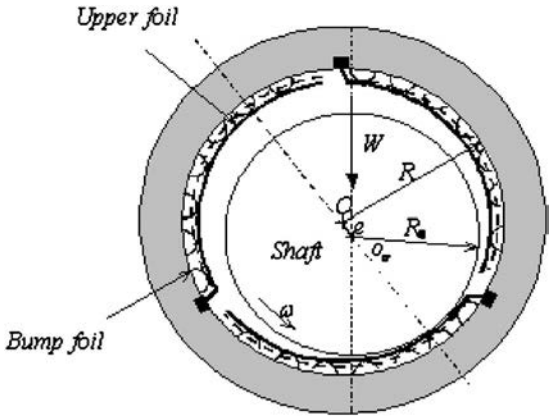

Fig. 5 Schematic of three lobed deformable bearing

engine failure speed and the static load seems to deviate from linear behavior and attain increasing polynomial nature.

Comments. In standard approaches the dynamic behavior of a deformable shaft supported by hydrodynamic bearings or ball bearings, is evaluated with the assumption that the bearing action is linear. The stiffness and damping matrix of the bearings are calculated and then introduced into a rotor dynamic computer code. This type of coupling is described as "weak." In the case of the aerodynamic bearings, we have been able to demonstrate that a linear dynamic analysis can lead to erroneous results according to the considered operation range.

The nonlinear character of a journal aerodynamic bearing is thus a significant fact to be considered in order to carry out an analysis of the rotor dynamic behavior. Therefore, we propose a "strong" coupling whereby the interaction of the bearings with the shaft is performed directly, step by step in time, in only one mode of the total calculation. In this first part the rotor was rigid and

Table 2 Main calculation characteristics for damping study

L/D	0.667
Number of pad	3
Pad angle, deg	110
Radial clearance, μm	50
Dimensionless compliance	0.2
$\alpha = \frac{C_c}{2\sqrt{KM}}$	0, 0.05, 0.1

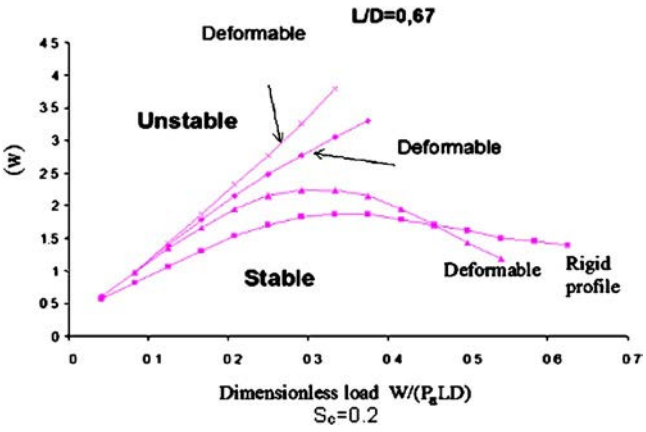

Fig. 6 Critical engine failure speed diagram for various values of α

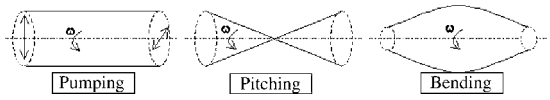

Fig. 7 Schematic representation of the considered vibration modes

symmetrically supported by two identical aerodynamic bearings.

It is now interesting to study the behavior of a more realistic case where the rotor is deformable and the bearings are not symmetrically mounted on the rotor. Because the approach presented is new, we have gradually proceeded towards the more complete problem of a deformable shaft with a nonlinear action of the journal aerodynamic bearings. Thus, the first part of the analysis consists of a dynamic model of a simple deformable rotor resulting from [14]. The Rayleigh-Ritz method with a three mode modal base is employed.

The dynamic behavior of a rotor mounted on two ball bearings was then compared to existing results for validation. Subsequently, the model was used to study the behavior of a deformable shaft running on two air bearings. The comparison with a linear "traditional" dynamic modeling confirmed once again the unique nonlinear dynamic behavior of the system. Finally, a comparison between a ball bearing and an air bearing points out the importance of the bearings on the overall dynamic behavior.

Rotor Dynamic Study With Foil Bearings

Short Description of the Rayleigh-Ritz Model. The Rayleigh-Ritz model uses a modal base restricted to three simple modes: pumping (or translation), pitching (or swinging), and first bending, Fig. 7. This modeling constitutes a first approach taking into account the two rigid body modes and the first bending mode of the shaft [54].

The symbol $R_0\ (X, Y, Z)$ indicates the initial frame (Fig. 8), in which the rotor axis at rest lies along the Y direction. The rotational speed Ω is considered constant. The rotor is considered as a beam and the neutral fiber displacement is studied. Each point on this fiber has two degrees of freedom that are displacements in the X and Z directions.

The expressions of the shaft neutral fiber displacements in the X and Z directions are, respectively, written in the following form:

$$u(y,t) = f_a(y)q_1(t) + f_b(y)q_3(t) + f_c(y)q_5(t) = f_a(y)q_1 + f_b(y)q_3 + f_c(y)q_5 \quad (6)$$

$$w(y,t) = f_a(y)q_2(t) + f_b(y)q_4(t) + f_c(y)q_6(t) = f_a(y)q_2 + f_b(y)q_4 + f_c(y)q_6 \quad (7)$$

where q_i are the generalized independent coordinates. The displacement functions, f_a, f_b, and f_c are, respectively, selected to represent the geometry of the vibration modes: pumping, pitching, and bending of a beam of constant section supported at its ends,

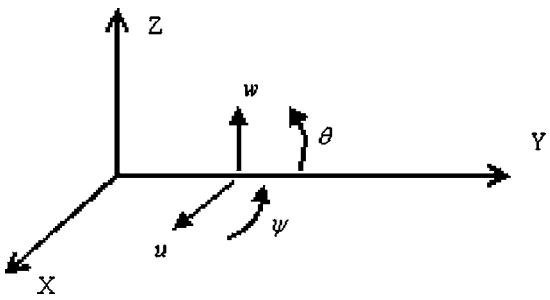

Fig. 8 Coordinate representation

$$f_a(y) = 1 \tag{8}$$

$$f_b(y) = 1 - \frac{2y}{L} \tag{9}$$

$$f_c(y) = \sin\frac{\pi y}{L} \tag{10}$$

The angular displacements ψ and θ of Fig. 8 are small and they can be approximated by

$$\theta = \frac{\partial w}{\partial y} = \frac{df_a(y)}{dy}q_2 + \frac{df_b(y)}{dy}q_4 + \frac{df_c(y)}{dy}q_6$$
$$= g_a(y)q_2 + g_b(y)q_4 + g_c(y)q_6 \tag{11}$$

and

$$\psi = -\frac{\partial u}{\partial y} = -\frac{df_a(y)}{dy}q_1 - \frac{df_b(y)}{dy}q_3 - \frac{df_c(y)}{dy}q_5$$
$$= -g_a(y)q_1 - g_b(y)q_3 - g_c(y)q_5 \tag{12}$$

The second order derivatives for u and w displacements are necessary to express the elastic energy of the shaft,

$$\frac{\partial^2 u}{\partial y^2} = \frac{d^2 f_a(y)}{dy^2}q_1 + \frac{d^2 f_b(y)}{dy^2}q_3 + \frac{d^2 f_c(y)}{dy^2}q_5$$
$$= h_a(y)q_1 + h_b(y)q_3 + h_c(y)q_5 \tag{13}$$

$$\frac{\partial^2 w}{\partial y^2} = \frac{d^2 f_a(y)}{dy^2}q_2 + \frac{d^2 f_b(y)}{dy^2}q_4 + \frac{d^2 f_c(y)}{dy^2}q_6$$
$$= h_a(y)q_2 + h_b(y)q_4 + h_c(y)q_6 \tag{14}$$

One may observe from the above expressions that $g_a(y)=0$ and $h_a(y)=0$ because f_a is of zero order. In the same way, $h_b(y)=0$ because f_b is of order one.

In the calculations below, we will not entirely develop the equations because manipulations are extensive but straightforward. We point out the expressions of various energies which should be calculated to write the Lagrange equations system [53].

Disk Element. The disk is considered as symmetrical. Its kinetic energy T_D can be written in the following way:

$$T_D = \frac{1}{2}M_D(\dot{u}^2 + \dot{w}^2) + \frac{1}{2}I_{Dx}(\dot{\theta}^2 + \dot{\psi}^2) + \frac{1}{2}I_{Dy}(\Omega^2 + 2\Omega\dot{\psi}\theta) \tag{15}$$

The energy of deformation of the disk is nil since it is considered as being rigid.

Rotor Element. The rotor elements are considered to be axisymmetric. The expression of kinetic energy T_S is as follows:

$$T_S = \frac{\rho S}{2}\int_0^L (\dot{u}^2 + \dot{w}^2)dy + \frac{\rho I}{2}\int_0^L (\dot{\theta}^2 + \dot{\psi}^2)dy + \rho IL\Omega^2$$
$$+ 2\rho I\Omega\int_0^L \dot{\psi}\theta dy \tag{16}$$

As the term $\rho IL\Omega^2$ is constant, we do not have to introduce this term in the writing of the Lagrange equations. The energy of deformation of the shaft, U_S is written as

$$U_S = \frac{EI}{2}\int_0^L \left[\left(\frac{\partial^2 u}{\partial y^2}\right)^2 + \left(\frac{\partial^2 v}{\partial y^2}\right)^2\right]dy \tag{17}$$

As the functions h_a and h_b are nil, the expression of the energy of deformation of the shaft is written according to the generalized coordinates,

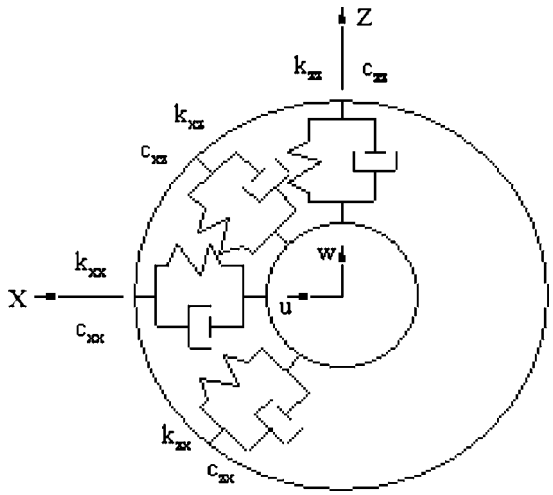

Fig. 9 Stiffness and damping coefficients of a ball bearing

$$U_S = \frac{EI}{2}\int_0^L h_c^2(y)dy(q_5^2 + q_6^2) \tag{18}$$

Unbalance. The shaft can be unbalanced. This unbalance is defined by a mass m_u at a distance d to the geometric center of the shaft. Its kinetic energy is written as

$$T_u = m_u d\Omega(\dot{u}\cos\Omega t - \dot{w}\sin\Omega t) \tag{19}$$

Having presented the energies, it is now appropriate to look at the actions of the ball bearings and/or the air bearings. In addition, to represent the operation of a shaft on air bearings, the influence of gravity must be added to the equations.

Ball Bearings. The shaft can possibly be supported by ball bearings. Their stiffness and damping coefficients are assumed to be known. The influence of the deflection is neglected, Fig. 9. The expression of the forces' virtual work exerted on the shaft is written in the following way:

$$\delta W_{rlt} = -k_{xx}u\delta u - k_{xz}w\delta u - k_{zz}w\delta w - k_{zx}u\delta w - c_{xx}\dot{u}\delta u - c_{xz}\dot{w}\delta u$$
$$- c_{zz}\dot{w}\delta w - c_{zx}\dot{u}\delta w \tag{20}$$

or

$$\delta W_{rlt} = F_{rltx}\delta u + F_{rltz}\delta w \tag{21}$$

where F_{rltx} and F_{rltz} are the components of the generalized forces of the ball bearing. In matrix form it can be written as

$$\begin{bmatrix} F_{rltx} \\ F_{rltz} \end{bmatrix} = -\begin{bmatrix} k_{xx} & k_{xz} \\ k_{zx} & k_{zz} \end{bmatrix}\begin{bmatrix} u \\ w \end{bmatrix} - \begin{bmatrix} c_{xx} & c_{xz} \\ c_{zx} & c_{zz} \end{bmatrix}\begin{bmatrix} \dot{u} \\ \dot{w} \end{bmatrix} \tag{22}$$

Air Bearings. Taking the air bearings into account in the behavior of a shaft requires the expression of the virtual work due to these bearings. As presented previously, the forces generated by the air bearings on the shaft depend at the same time on the local deflection of the rotor on the level of each bearing as well as the rotational speed. The expression of the virtual work of the forces generated by an air bearing is as follows:

$$\delta W_{pal} = F_{palx}\delta u + F_{palz}\delta w \tag{23}$$

with F_{palx}, F_{palz}, the components of the forces generated by the air bearing on the rotor. The components of the forces generated by the bearing are calculated at each time step, using Reynolds equation expressed in dynamic regime (Eq. (5)).

The Reynolds equation provides the field pressure which leads, upon integration, to the fluid film forces acting in the bearing. This kind of coupling is detailed in [26] in the case of a rigid rotor

symmetrically supported by two air bearings. In order to simplify calculations, we do not consider misalignment of the bearing generated by pitching, bending of the shaft or a difference in value of the magnitude of the static loads applied to the bearings.

Gravity. The action of gravity creates an offset of the rotor in the air bearings. We consider that the total mass of the shaft exerts a force located at the shaft center of gravity. The expression of the virtual work due to gravity is as follows:

$$\delta W_{\text{gravity}} = - M_{\text{total}} g \, \delta w(y_{cdg}) \tag{24}$$

with M_{total} as the total mass of the shaft, g is the acceleration of gravity, and y_{cdg} is the Y-coordinate of the shaft's center of gravity.

We obtain the system of equations by application of the Lagrange formalism,

$$\frac{d}{dt}\left(\frac{\partial T_c}{\partial \dot{q}_i}\right) - \frac{\partial T_c}{\partial q_i} + \frac{\partial U}{\partial q_i} = \delta W_i \tag{25}$$

with $i=1-6$, T_c being the kinetic energy, U the energy deformation of the whole shaft components, δW the total virtual work, and q_i the generalized coordinates of the system. Thus we can obtain the system of equations for the rotor dynamic which can be written in the following matrix form,

$$[M]\{\ddot{q}\} + [C]\{\dot{q}\} + [K]\{q\} = \{F\} \tag{26}$$

with $[M]$ the matrix of mass, $[C]$ the matrix governing the gyroscopic effect and possibly the ball bearing damping, $[K]$ the matrix of the rotor stiffness and possibly the ball bearing stiffness, $\{F\}$ the vector of the external actions (the unbalance, the air bearings forces and gravity).

Dimensionless Equations. The system of equations can be written in the following form:

$$[\overline{M}]\{\overline{\ddot{Q}}\} + \frac{1}{\Omega}[\overline{C}]\{\overline{\dot{Q}}\} + \frac{1}{\rho L^3 \Omega^2}[\overline{K}]\{\overline{Q}\} = \{\overline{F}\} \tag{27}$$

with the following dimensionless variable definitions:

$$\overline{Q_i} = \frac{q_i}{C_0},\ \overline{\dot{Q}_i} = \frac{\dot{q}_i}{C_0\Omega},\ \overline{\ddot{Q}_i} = \frac{\ddot{q}_i}{C_0\Omega^2},\ [M],\ \overline{M_{ij}} = \frac{M_{ij}}{\rho L^3},$$

$$\overline{C_{ij}} = \frac{C_{ij}}{\rho L^3},\ \overline{F_i} = \frac{F_i}{\rho L^3 C_0 \Omega^2} \tag{28}$$

with time $T=t\Omega$, Ω as the rotational speed. The parameter C_0 denotes an arbitrary value of the order of the bearing radial clearance. The symbols δ and L, respectively, denote the density and the length of the rotor.

This dynamic system must be solved step by step in time to take into account the nonlinear variations of aerodynamic bearing forces in the right hand side member. The numerical integration scheme is the same as that presented in [26].

Validation

The results from the model are compared to those given in [14] for a rotor described in Fig. 10, supported by two ball bearings (Table 3). In the reference, the rotor is modeled by finite element method with a pseudo-modal reduction.

Four critical speeds are given by the Rayleight Ritz model (Table 4). The first two critical speeds are very close to the reference value, Fig. 11. The last two critical speeds are quite different. In this case, modes three and four involve bending modes that are more complex than the first bending mode involved in the Rayleigh-Ritz model. The first two modes are the first bending mode. This study confirms that the simplified Rayleigh-Ritz model gives good results if the rotor bending mode remains simple. Generally, the rotors used in oil-free turbomachinery are quite stiff, thus considering only rigid and first bending modes is a reasonable assumption.

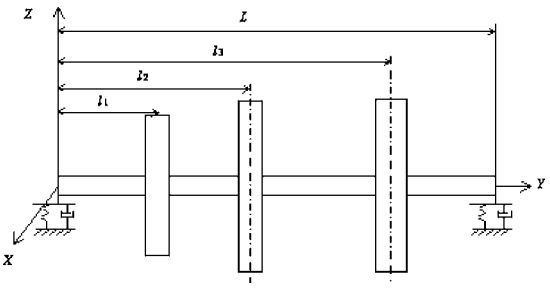

Fig. 10 Configuration of the reference case

Results and Discussion

The Rayleigh-Ritz model will now be used to study the dynamic behavior of a deformable shaft supported by air bearings. Thus we will be able to show the usefulness of this type of analysis while observing, in particular, the influence of the rotor flexibility on the response to an unbalance and the stability threshold of the system. We consider a solid or hollow shaft of external length 300 mm and 50 mm of diameter, as shown in Fig. 12. In the speed range of 2000–18,000 rpm, the dynamic behavior is close to the symmetrical rigid configuration (Fig. 13). This rotor seems too short and thus too stiff to observe deflection phenomena in the considered speed range. Once again this validates the Rayleigh-Ritz model. The influence of the bending mode has not been shown by this example.

To increase the bending mode, a rotor with 900 mm length is chosen for the rest of the study. The air bearings, as in the preceding case, are located at 50 mm from the ends of the rotor. The dynamic calculation of this shaft's behavior with nonlinear action of the air bearings gives an interesting response curve to unbalance. We always observe a peak of amplitude towards 4000 rpm. It is similar to the case of a rigid rotor but a second peak appears towards 9500 rpm. We compare this response curve in Fig. 14 with that obtained from the symmetrical rigid rotor simple model in order to highlight the effect of the rotor's flexibility.

It is interesting to represent the deformation of the rotor for speeds of 4000 and 9500 rpm, Figs. 15 and 16. These figures give the representation of the trajectory of the rotor's center for various Y-coordinates. We took the precaution to remove the static deformation of the shaft due to gravity, so that the observation of the deformation in rotation is easier.

It appears clearly that the mode of vibration at the speed of 4000 rpm is of the "rigid body" type because we obtain a very small twist of the shaft. The amplitude of displacements along the Z-axis is one third of those along the X-axis, Fig. 15.

For the speed of 9500 rpm, the associated mode of vibration introduces the inflection of the rotor whose form is complex. It should be noted that the amplitude of the deformation along the Z-axis (direction of the weight) is approximately four times higher than that in the X-direction, Fig. 16.

One can also plot on the same graph the response curves to unbalance in configuration ball bearings and air bearings, Fig. 17. It appears that the two curves present notable differences. First of all, we note that the air damping of the bearings leads to a decrease of the amplitude of the rotor center trajectory compared that of a "ball bearing" configuration (with identical unbalance). At high speed, the eccentricity is low, film thickness is high, and the air bearing stiffness is less than that of a classical ball bearing. Hence, a part of the second mode energy is in the bearing and not in the rotor, as with ball bearings. In the air bearing configuration, we thus obtain displacements which are due to both the rigid and

Table 3 Data for the reference case

	$l_1=0.2$ m, $l_2=0.5$ m, $l_3=1$ m, $L=1.3$ m		
Rotor	Plain section, $\phi=0.05$ m $E=2\times10^{11}$ N/m^2, $\rho=7800$ kg/m^3, $\nu=0.3$		
Disk	Thickness, m	Inner diam, m	Outer diam, m
Disk 1 (l_1)	0.05	0.05	0.12
Disk 2 (l_2)	0.05	0.05	0.2
Disk 3 (l_3)	0.06	0.05	0.2
Bearing stiffness and damping	$K_{xx}=5\times10^7$ N/m, $K_{zz}=7\times10^7$ N/m, $K_{xz}=K_{zx}=0$ $C_{xx}=5\times10^2$ N/m/s, $C_{zz}=7\times10^2$ N/m/s, $C_{xz}=C_{zx}=0$		
Unbalance	200 g mm on disk 2		
Velocity	from 0 to 30000 rpm		

bending modes. At low speed, a rigid vibration mode is present with the air bearing configuration and not with that of the ball bearings. This simple case outlines how bearings influence the whole dynamic response of the system.

General Conclusions

This study of aerodynamic journal bearing dynamic characteristics has been conducted because it is crucial to understanding rotor dynamic behavior. Initially, the rotor is considered to be rigid and supported symmetrically by two identical radial bearings. We have shown that the linear modeling, i.e., representing the bearings with stiffness and damping coefficients, has a restricted field of validity. For instance, in the case of a three lobe rigid bearing without geometrical preload, this range is limited to relative eccentricities lower than 0.65.

Thus, the prediction of the bearing stability threshold and the response to dynamic excitations can be erroneous if one uses a linear approach beyond the appropriate limit for this type of aerodynamic bearing. In addition, we illustrated the fact that for high loads the deformable bearing profiles have a lower stability than their rigid counterparts. Since we were fully aware that this observation goes against some physical phenomena observed in experiments, we set up a model which takes into account a structural damping of viscous type in the nonlinear approach. Even with very low coefficient values of the bearing structural damping, the level of stability could be increased, in accordance with the phenomena presented in the literature.

Having clearly highlighted the nonlinear character of aerodynamic bearings dynamic behavior, we considered direct coupling with a deformable shaft. At this point we developed a calculation

Table 4 Critical speeds

	Critical speed, Rayleigh-Ritz rpm	Critical speed, Reference rpm
1	3610	3620
2	3840	3798
3	12850	10018
4	15080	11279
5	...	16785
6	...	24408
7	...	26615

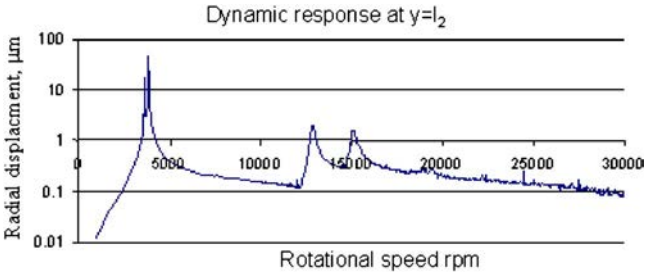

Fig. 11 Dynamic response at $y=l_2$

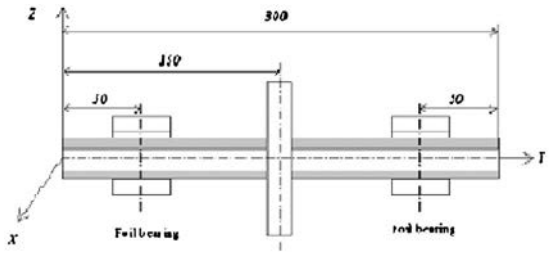

Fig. 12 Scematic of a hollow shaft with a central disk

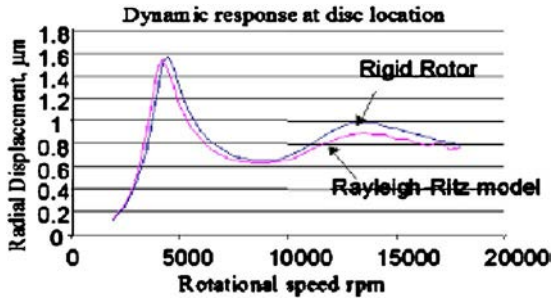

Fig. 13 Comparison between the Rayleigh-Ritz model and rigid rotor model

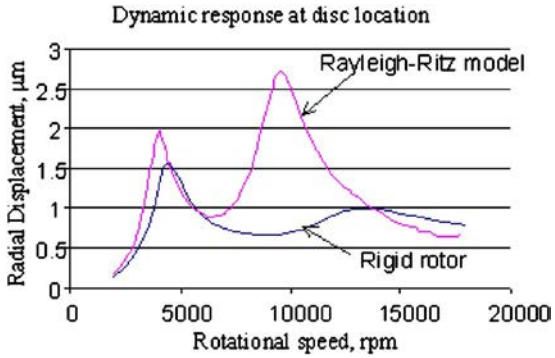

Fig. 14 Response curve to unbalance. Comparison with the rigid case.

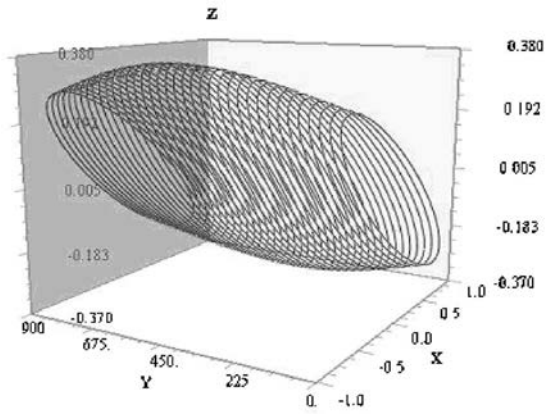

Fig. 15 Deformation of the rotor at 4000 rpm

based on the Rayleigh-Ritz method using a base of three modes (pumping, pitching, and bending). Thus, we were able to confirm the coherence of the obtained results compared to those from the rigid rotor model.

The deformation of the rotor reveals modes of vibrations which cannot be predicted by the rigid model. At low speed, a rigid mode of vibration is present with the air bearing configuration. At high speed we obtain displacements which are due to both rigid and bending modes. This simple case brought into light the influence of the bearing on the dynamic response of the complete system. It appears clearly in the first part of this paper that the addition of damping within the deformable structure leads to the increase of the deformable bearing's stability level.

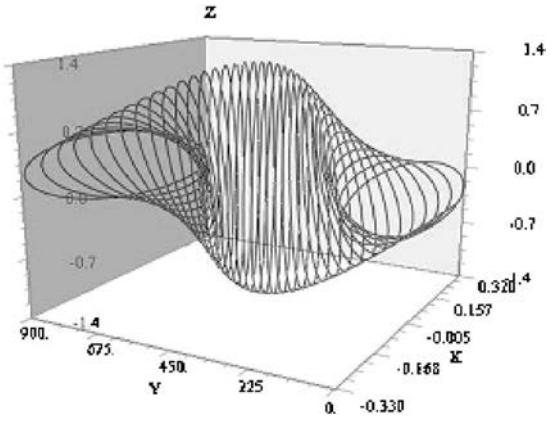

Fig. 16 Deformation of the rotor at 9600 rpm

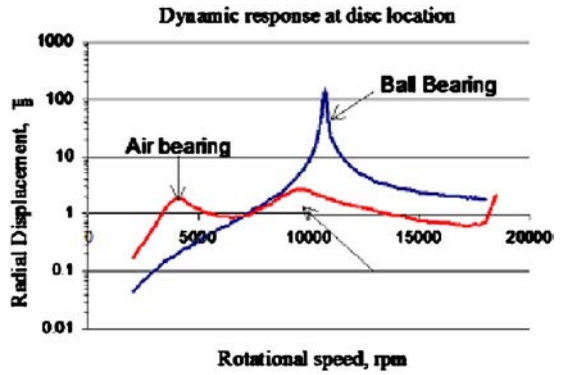

Fig. 17 Response curves to unbalance in configuration ball bearings, air bearings with linear and nonlinear action

As could be expected, the higher the damping coefficient, the higher the critical speed. Furthermore, the critical speed does not decrease further with load increase. The relation between the critical engine failure speed and the static load seems to deviate from linear behavior and approach a higher order polynomial form. It is clear that future work will relate on the one hand to the modeling of dry friction between the foils and the bumps to properly quantify the damping brought by this process, and on the other hand to the development of a more realistic rotor dynamic model so as to properly characterize the dynamic behavior of the whole system.

Nomenclature

C = radial clearance
C_{ij} = damping coefficients
D = bearing diameter
e = bearing eccentricity
E = Young modulus
$f_{a,b,c}$ = displacement functions
F_{rltx}, F_{rltz} = roller bearing forces
F_{palx}, F_{palz} = bearing forces
g = gravity acceleration
h = film thickness
H = dimensionless film thickness, $H=h/C$
I = rotor inertia in the X direction
I_{Dx} = disk inertia in the X direction
I_{Dy} = disk inertia in the Y direction
K_{ij} = bearing stiffness coefficients
K_s = stiffness coefficient of the structure
L = bearing length
M = rotor mass
M_D = disk mass
O = bearing center
O_a = shaft center
p = pressure
p_a = ambient pressure
P = dimensionless pressure, p/p_a
q_i = generalized coordinates
R = bearing radius
R_a = shaft radius
S_c = compliance
S = bearing section
$\overline{S_c}$ = dimensionless compliance $\overline{S}=S(P_a/C)$
t = time
T = dimensionless time, $T=t\omega$
T_S = rotor kinetic energy
T_D = disk kinetic energy
T_C = total kinetic energy
T_u = unbalance kinetic energy
U_1 = speed component in X direction
U_S = rotor energy deformation
$u(y,t)$, v, w = shaft displacement in the X, Y, and Z directions
X, Y, Z = initial frame
x, y, z = local frame
W_o = static load
W = carrying capacity
$\overline{W}$ = dimensionless carrying capacity, $\overline{W}=W/(p_aLD)$
$W_{dx,y}$ = external dynamic forces
δW = virtual work
α = damping coefficient
Ω, ω = rotational speed
Θ, Ψ = shaft angular displacements
Λ = bearing number

References

[1] Cameron, M., 1965, *The Principles of Lubrication*, Longmans Green Editions.

[2] Heshmat, H., Shapiro, W., and Gray, S., 1982 "Development of Foil Journal Bearings for High Load Capacity and High Speed Whirl Stability," J. Lubr. Technol., **104**, pp. 149–156.

[3] Heshmat, H., Walowit, A., and Pinkus, O., 1983, "Analysis of Gas-Lubricated Foil Journal Bearings," J. Lubr. Technol., **105**, pp. 647–655.

[4] Licht, L., and Branger, M., 1975, "Motion of a Small High—Speed Rotor in 3 Types of Foil Bearings," J. Lubr. Technol., **97**(2), pp. 270–282.

[5] Iordanoff, I., 1996, "Paliers Axiaux Aérodynamiques à Structure à Feuilles: Analyse et Optimisation," Ph.D. thesis, Université Paul Sabatier, Toulouse, France.

[6] Flamand, L., 1999, "Lubrification Hydrodynamique," GMD, Institut National des Sciences Appliquées de Lyon, France.

[7] Iordanoff, I., 1999, "Analysis of an Aerodynamic Compliant Foil Thrust Bearing: Method for a Rapid Design," ASME J. Tribol., **121**, pp. 816–822.

[8] Heshmat, H., Ming Chen, H., and Walton, J. F., 2000, "On the Performance of Hybrid Foil-Magnetic Bearings," ASME J. Eng. Gas Turbines Power, **122**, pp. 73–82.

[9] Salehi, M., and Heshmat, H., 2000, "On the Fluid and Thermal Analysis of a Compliant Surface Foil Bearing and Seal," Tribol. Trans., **43**, pp. 318–324.

[10] Yang, B. S., Lee, Y. H., Choi, B. K., and Kim, H. J., 2001, "Optimum Design of Short Journal Bearings by Artificial Life Algorithm," Tribol. Int., **34**, pp. 427–435.

[11] Stephan, P., and Iordanoff, I., 2001, "Butées et Paliers Aérodynamiques," Techniques de l'Ingénieur, B5335.

[12] Dellacorte, C., and Laskowski, A., 1997, "Tribological Evaluation of PS300: A New Chrome Oxide-Based Solid Lubricant Coating Sliding Against Al_2O_3 From 25° to 650°C," Tribol. Trans., **40**, pp. 163–167.

[13] Dellacorte, C., 1998, "A New Foil Air Bearing Test Rig for Use to 700°C and, 70,000 rpm," Tribol. Trans., **41**, pp. 335–340.

[14] Dellacorte, C., Fellenstein, J. A., and Benot, P. A., 1999, "Evaluation of Advanced Solid Lubricant Coatings for Foil Air Bearings Operating at 25 and 500°C," Tribol. Trans., **42**, pp. 338–342.

[15] Suriano, F. J., Keiser, R. J., Woessner, F. G., and Valori, R., 2001, "High-Temperature (649°C/1200°F) Coatings for Gas-Lubricated Foil Bearings of the Navy's Advanced Auxiliary Power Unit Concepts," Garret Turbine Engine Company and Naval Air Propulsion Cente report.

[16] Herbelot, C., 1995, "Comportement Stationnaire ou Dynamique de Paliers Aérodynamiques à Feuilles," Ph.D. thesis, Universite Paul Sabatier, Toulouse, France.

[17] Boedo, S., and Eshkabilov, S. L., 2003, "Optimal Shape Design of Steadily Loaded Journal Bearings using Genetic Algorithms," Tribol. Trans., **46**, pp. 134–143.

[18] Roger KU, C. P., and Heshmat, H., 1993, "Compliant Foil Bearing Structural Stiffness Analysis, Part II: Experimental Investigation," ASME J. Tribol., **115**, pp. 364–369.

[19] Heshmat, H., 1994, "Advancements in the Performance of Aerodynamic Foil Journal Bearings: High Speed and Load Capability," ASME J. Tribol., **116**, pp. 287–295.

[20] Carpino, M., Peng, J. P., and Medvetz, L., 1994, "Misalignment in a Complete Shell Gas Foil Journal Bearing," Tribol. Trans., **37**, pp. 829–835.

[21] Carpino, M., Peng, J. P., and Medvetz, L., 1994, "Effects of Membrane Stresses in the Prediction of Foil Bearing Performance," Tribol. Trans., **37**, pp. 43–50.

[22] Heshmat, H., and Heshmat, C. A., 1995, "An Analysis of Gas-Lubricated, Multileaf Foil Journal Bearings With Backing Springs," ASME J. Tribol., **117**, pp. 437–443.

[23] Czolczynski, K., and Marynowski, K., 1996, "Stability of Symmetrical Rotor Supported in Flexibly Mounted, Self-Acting Gas Journal Bearings," Wear, **194**, pp. 190–197.

[24] Czolczynski, K., 1996, "How to Obtain Stiffness and Damping Coefficients of Gas Bearings," Wear, **201**, pp. 265–275.

[25] Howard, S. A., 1999, "Preliminary Development of Characterization Methods for Compliant Air Bearings," Tribol. Trans., **42**, pp. 789–794.

[26] Heshmat, H., 2000, "Operation of Foil Bearings Beyond the Bending Critical Mode," ASME J. Tribol., **122**, pp. 192–198.

[27] Howard, S. A., Dellacorte, C., Valco, M. J., Prahl, J. M., and Heshmat, H., 2001, "Steady-State Stiffness of Foil Air Journal Bearings at Elevated Temperatures," Tribol. Trans., **44**, pp. 489–493.

[28] Howard, S. A., Dellacorte, C., Valco, M. J., Prahl, J. M., and Heshmat, H., 2001, "Dynamic Stiffness and Damping Characteristics of a High-Temperature Air Foil Journal Bearing," SLTE presentation, preprint No. 01-TC-7.

[29] Lee, N. S., Choi, D. H., Lee, Y. B., Kim, T. H., and Kim, C. H., 2002, "The Influence of the Slip Flow on Steady—State Load Capacity, Stiffness and Damping Coefficients of Elastically Supported Gas Foil Bearings," Tribol. Trans., **45**, pp. 478–484.

[30] Yoshimoto, S., and Nakano, Y., 1983, "Stability of Unsymmetrical Rigid Rotor Supported by Self-Acting Gas-Lubricated Journal Bearings," J. Lubr. Technol., **105**, pp. 656–661.

[31] Abdul Wahed, N., Nicolas, D., and Pascal, M. T., 1982, "Stability and Unbalance Response of Large Turbine Bearings," J. Lubr. Technol., **104**, pp. 66–75.

[32] Klit, P., and Lund, W., 1986, "Calculation of the Dynamic Coefficients of a Journal Bearing, Using a Variational Approach," ASME J. Tribol., **108**, pp. 421–425.

[33] Stephan, P., 1991, "Paliers à Gaz à Alésage Expansible, Comportement Dynamique," Ph.D. thesis, Université Paul Sabatier, Toulouse, France.

[34] Carpino, M., and Peng, J. P., 1993, "Calculation of Stiffness and Damping Coefficients for Elastically Supported Gas Foil Bearings," ASME J. Tribol., **115**, pp. 20–27.

[35] Abdul Wahed, N., 1982, "Comportement Dynamique des Paliers Fluides. Etude Linéaire et Nonlinéaire," Ph.D. thesis, INSA de Lyon, France.

[36] Hsia, Y. T., and Domoto, G. A., 1983, "An Experimental Investigation of Molecular Rarefaction Effects in Gas Lubricated Bearings at Ultra-Low Clearances," J. Lubr. Technol., **105**, pp. 120–130.

[37] Frene, J., Nicolas, D., Berthe, D., and Berthe, D., 1990, *Lubrification Hydrodynamique, Paliers et Butées*, edition Eyrolles.

[38] Tichy, J., and Bou-Saïd, B., 1991, "Hydrodynamic Lubrication and Bearing Behaviour With Impulsive Loads," Tribol. Trans., **34**, pp. 505–512.

[39] Li, D. F., Choy, K. C., and Allaire, P. E., 1980, "Stability and Transient Characteristics of Four Multilobe Journal Bearing Configurations," J. Lubr. Technol., **102**, pp. 291–299.

[40] Li, D. F., Choy, K. C., and Allaire, P. E., 1980, "Transient Unbalance Response of Four Multilobe Journal Bearings," J. Lubr. Technol., **102**, pp. 300–306.

[41] Jai, M., Buscaglia, G., and Iordanoff, I., 2004, "Multi-Constrained Optimization of Running Characteristics of Mechanisms Lubricated With Compressible Fluid," ASME J. Tribol., **126**, pp. 126–132.

[42] Buscaglia, G., and Jai, M., 2001, "A New Numerical Scheme for Nonuniform Homogenized Problems: Application to the Nonlinear Reynolds Compressible Equation," Math. Probl. Eng., **7**(4), pp. 355–377.

[43] Bonneau, O., 1989, "Comportement Statique et Dynamique de Ligne d'Arbre Montée sur Paliers Fluides: Influence des Caractéristiques des Paliers," Ph.D. thesis, Universite de Poitiers, France.

[44] Nrakis, Y., and Cohen, M. J., 1977, "Response of Infinite Journal Gas Bearings to Harmonic Perturbations in the Rotational Speed," J. Lubr. Technol., **99**(4), pp. 428–433.

[45] Braun, M. J., Choy, F. K., Dzodzo, M., and Hsu, J., 1996, "Two-Dimensional Dynamic Simulation of a Continuous Foil Bearing," Tribol. Int., **29**, pp. 61–68.

[46] Howard, S. A., 1999, "Rotordynamics and Design Methods of an Oil-Free Turbocharger," Tribol. Trans., **42**, pp. 174–178.

[47] Carpino, M., and Peng, J. P., 1994, "Coulomb Friction Damping Effects in Elastically Supported Gas Foil Bearings," Tribol. Trans., **37**, pp. 91–98.

[48] Roger, C. P., and Heshmat, H., 1992, "Compliant Foil Bearing Structural Stiffness Analysis, Part I: Theoretical Model Including Strip and Variable Bump Foil Geometry," ASME J. Tribol., **114**, pp. 394–400.

[49] Roger KU, C. P., and Heshmat, H., 1994, "Structural Damping of Self-Acting Compliant Foil Journal Bearings," ASME J. Tribol., **116**, pp. 76–82.

[50] Roger KU, C. P., and Heshmat, H., 1994, "Structural Stiffness and Coulomb Damping in Compliant Foil Journal Bearings: Theoretical Considerations," Tribol. Trans., **37**, pp. 525–533.

[51] Arakere, N., and Nelson, H. D., 1988, "An Interior Collocation Method for Static and Dynamic Analysis of Finite Length Gas Journal Bearings," ASME J. Tribol., **110**, pp. 456–461.

[52] Grau, G., Iordanoff, I., Bou-Saïd, B., and Berthier, Y., 2004, "An Original Definition of the Profile of Compliant Foil Journal Bearings: Static and Dynamic Analysis," Tribol. Trans., **47**, pp. 1–9.

[53] Lalanne, M., and Ferraris, G., 1998, *Rotordynamics Prediction in Engineering*, 2nd ed., Wiley, NY.

[54] Lalanne, M., Berthier, P., and Der Hagopian, J., 2000, *Mechanical Vibrations for Engineers*, Wiley, NY.